

# A Novel Range Finding System Using Correlation Image Sensor

Member Akira Kimachi (The University of Tokyo)  
 Non-member Toru Kurihara (The University of Tokyo)  
 Non-member Masao Takamoto (The University of Tokyo)  
 Member Shigeru Ando (The University of Tokyo)

This paper proposes a 3-D measurement principle for the correlation image sensor (CIS) which generates temporal correlation between incident light intensity and an external reference signal at each pixel. Another key of our system besides the CIS is amplitude modulation of the scanning sheet beam, the phase of which relative to a reference signal is varied according to the angle of the sheet beam. After a scan within a frame, the phase is demodulated with a quadrature pair of reference signals and output by the CIS to compute the individual angle of the sheet beam on each pixel. By virtue of the lock-in detection principle, effects of background illumination and/or surface reflectance nonuniformity of the object are thoroughly removed. We implemented this system using our CMOS 64×64-pixel CIS, and successfully reconstructed a depth map under its frame rate (30Hz).

**Keywords:** range finder, 3-D profile, lock-in detection, CMOS, correlation image sensor, vision chip

## 1. Introduction

Three-dimensional (3-D) measurement or range finding<sup>(1)</sup> has been an important issue in machine vision applications such as inspection, industrial assembly and vehicle navigation. Among a number of range finding methods, light-stripe methods have widely been used, in which the depth of an object is determined from the projection angle and cross section image of a sheet beam by triangulation. Conventional light-stripe methods use a sequence of cross section images while scanning the sheet beam step by step, but a large number of images are required to increase the spatial resolution of a range data, which, in turn, decreases the speed of the whole system. Another problem lies in the image processing for detecting stripe location, which decreases measurement speed and spatial resolution.

These problems can be avoided if the beam angle is directly determined at each pixel. This motivated development of special VLSI sensors for the light-stripe method. Gruss *et al.*<sup>(2)</sup> proposed a sensor that records timestamps by latching a ramp signal at the moment when integrated photocarriers exceed a threshold. Kang *et al.*<sup>(3)</sup> used a digital counter instead of an analog timestamp signal. These sensors can, however, be affected by background illumination or surface reflectance nonuniformity of the object owing to the uniform threshold. To overcome this problem, Yokoyama *et al.*<sup>(4)</sup> introduced a differential detection principle of the moment using a pair of photodiodes within each pixel. But the improvement is restricted for smooth disturbances alone.

This paper proposes a light-stripe range finder using the time-domain correlation image sensor (CIS). The

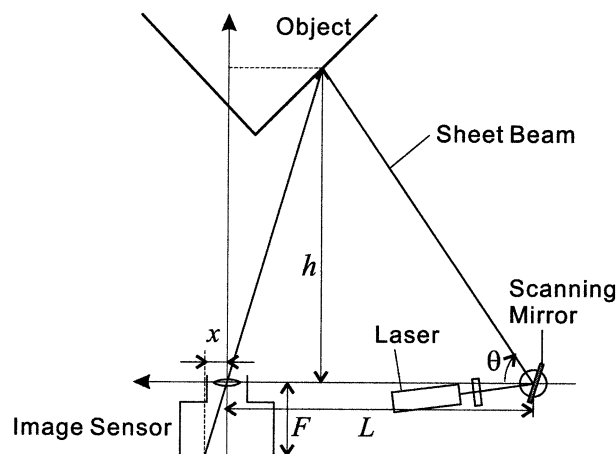


Fig. 1. Geometry of light-stripe range finding.

CIS, proposed by us<sup>(5)-(8)</sup>, produces temporal correlation between incident light intensity  $f_{ij}(t)$  and a pixel-common reference signal  $g(t)$  at each pixel:

$$\phi_{ij}(t) = \langle f_{ij}(t)g(t) \rangle = \int_{t-T}^t f_{ij}(\tau)g(\tau)d\tau, \dots (1)$$

where  $T$  denotes the frame interval. The most remarkable difference of our method from the conventional timestamp-type sensors is that the angle of the sheet beam is encoded in the modulation phase of the beam intensity and demodulated on each pixel by the correlation image sensor. Recovering the phase based on the correlation detection principle has advantages of removing the effect of background illumination and surface reflectance nonuniformity. The following part of this paper describes the sensing principle and the sensing system we have developed using a 64×64-pixel

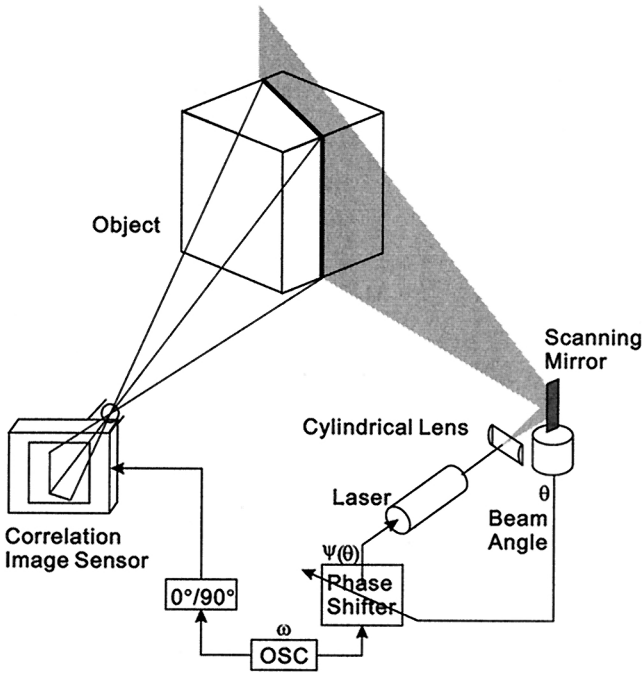


Fig. 2. Schematic of the range finding method using the CIS.

sensor<sup>(9)(10)</sup>, and shows experimental results obtained on the sensing system.

## 2. Principle of Range Measurement Using CIS

Fig. 1 depicts the geometry of a typical light-stripe range finder, in which the depth of an object,  $h(x, y)$ , is determined from the projection angle  $\theta$  of the sheet beam and the  $x$ -coordinate of the cross section of the beam:

$$h(x, y) = \frac{L}{\frac{x}{F} + \frac{1}{\tan \theta}}, \dots \dots \dots (2)$$

where  $F$  denotes the effective focal length of the camera (distance from the lens center to the image sensor) and  $L$  the distance (baseline length) between the lens center of the image sensor and the axis of the scanning mirror.

In this paper we consider the system of Fig. 2. The laser sheet beam is amplitude-modulated at frequency  $\omega_m$  and scans the object with time-varying angle  $\theta(t)$ . The phase  $\psi$  of this modulation is designed to vary as a monotonic function of the beam angle  $\theta(t)$ . Let us express this modulation as  $\cos[\omega_m t - \psi(\theta(t))]$ . In a single scan of the beam over a frame interval  $T$ , each pixel of the correlation image sensor produces temporal correlation between incident light intensity  $f_{ij}(t)$  and quadrature reference signals  $\cos \omega_m t$  and  $\sin \omega_m t$ . In the presence of background illumination and surface reflectance nonuniformity of the object, the incident light intensity  $f_{ij}(t)$  at pixel  $(i, j)$  can be written as

$$f_{ij}(t) = \begin{cases} R_{ij}[I_{ij}^0(t) + I_{ij}\{1 + m \cos[\omega_m t - \psi(\theta(t))]\}], & t \in [t_{ij}^1, t_{ij}^2], \\ R_{ij}I_{ij}^0(t), & \text{otherwise,} \end{cases} \quad (3)$$

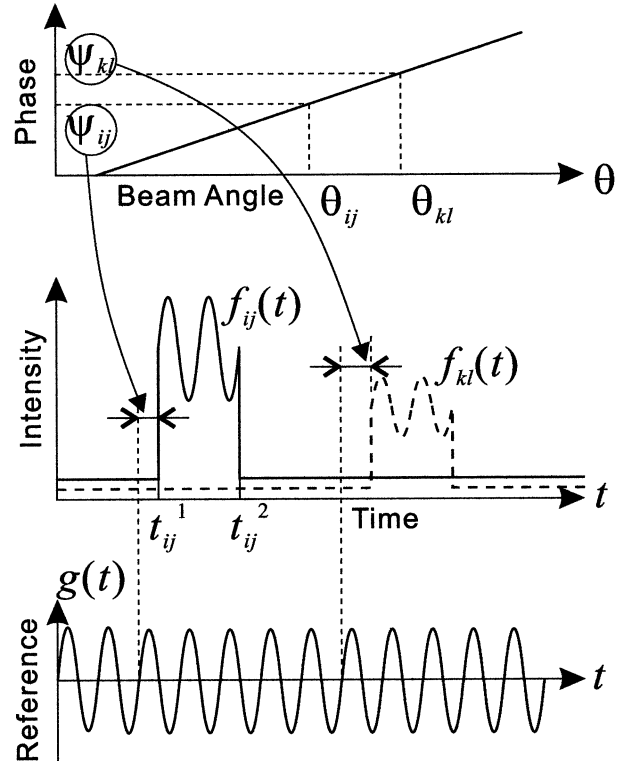


Fig. 3. Relationship among light intensity  $f_{ij}(t)$ , reference signal  $g(t)$ , phase  $\psi$  and beam angle  $\theta(t)$ .

where  $R_{ij}$  denotes the surface reflectance coefficient,  $I_{ij}^0(t)$  the intensity of background illumination,  $I_{ij}$  the dc-level intensity of the sheet beam,  $m$  the modulation amplitude relative to  $I_{ij}$  (modulation depth), and  $[t_{ij}^1, t_{ij}^2]$  the time interval within which the stripe image sweeps the pixel  $(i, j)$  (Fig. 3). Here the phase  $\psi(\theta(t))$ , sweep interval  $[t_{ij}^2, t_{ij}^1]$  and modulation frequency  $\omega_m$  are chosen so that they satisfy the following:

- (1)  $\psi(\theta(t))$  is approximately constant for  $t \in [t_{ij}^1, t_{ij}^2]$ , i.e.  $\psi(\theta(t)) \simeq \psi_{ij}$ .
- (2) A sufficiently large number of waves is captured for  $t \in [t_{ij}^1, t_{ij}^2]$  so that  $\frac{\omega_m}{2\pi}(t_{ij}^2 - t_{ij}^1) \gg 1$  is satisfied.
- (3)  $\cos \omega_m t$  and  $\sin \omega_m t$  are uncorrelated with the background illumination  $I_{ij}^0(t)$ , i.e.  $\int_0^T I_{ij}^0(t) \cos \omega_m t dt \simeq 0$ ,  $\int_0^T I_{ij}^0(t) \sin \omega_m t dt \simeq 0$ .

Using a reference signal  $g(t) = \cos \omega_m t$ , the output from pixel  $(i, j)$  of the CIS is then computed as

$$\begin{aligned} \phi_{ij}^1 &\equiv \int_0^T f_{ij}(\tau) \cos \omega_m \tau d\tau \\ &= R_{ij} \int_0^T I_{ij}^0(\tau) \cos \omega_m \tau d\tau \\ &\quad + R_{ij} I_{ij} \int_{t_{ij}^1}^{t_{ij}^2} \{1 + m \cos[\omega_m \tau - \psi(\theta(\tau))]\} \\ &\quad \cdot \cos \omega_m \tau d\tau. \dots \dots \dots (4) \end{aligned}$$

The first term vanishes since  $I_{ij}^0(t)$  is uncorrelated with  $\cos \omega_m t$ . The second term, under the assumption of  $\psi(\theta(t)) \simeq \psi_{ij}$  for  $t \in [t_{ij}^1, t_{ij}^2]$ , is rearranged as

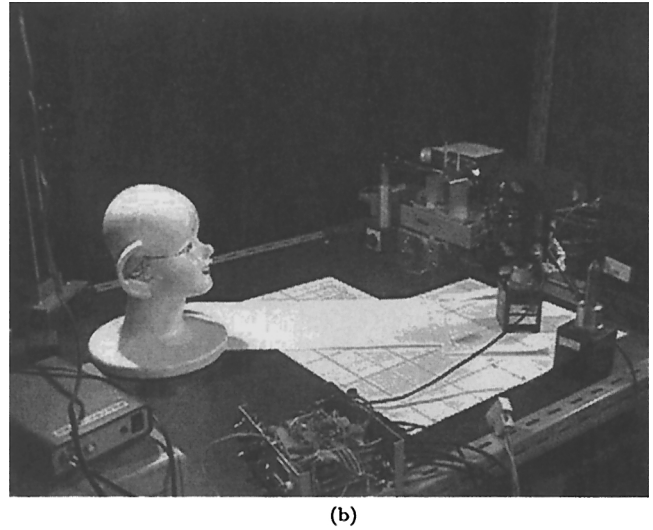
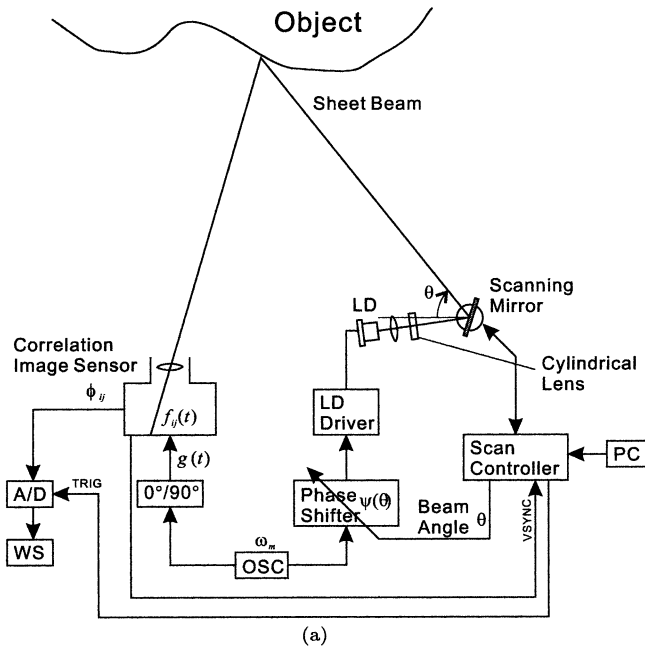


Fig. 4. (a) Schematic diagram of the experimental system. (b) Photograph of the system.

$$\begin{aligned}
 & A_{ij} \cos \psi_{ij} \\
 & + A_{ij} \left\{ \frac{2}{m} \operatorname{sinc} \frac{\omega_m}{2} (t_{ij}^2 - t_{ij}^1) \cos \frac{\omega_m}{2} (t_{ij}^2 + t_{ij}^1) \right. \\
 & \left. + \operatorname{sinc} \omega_m (t_{ij}^2 - t_{ij}^1) \cos [\omega_m (t_{ij}^1 + t_{ij}^2) - \psi_{ij}] \right\} \quad (5)
 \end{aligned}$$

where

$$A_{ij} = \frac{1}{2} m R_{ij} I_{ij} (t_{ij}^2 - t_{ij}^1). \quad (6)$$

This term is reduced to  $A_{ij} \cos \psi_{ij}$  since  $\operatorname{sinc} [\omega_m (t_{ij}^2 - t_{ij}^1)] \ll 1$  and  $\operatorname{sinc} [\frac{\omega_m}{2} (t_{ij}^2 - t_{ij}^1)] \ll 1$  for  $\frac{\omega_m}{2\pi} (t_{ij}^2 - t_{ij}^1) \gg 1$  by assumption. Thus we finally obtain only the phase term in the correlation output

$$\phi_{ij}^1 \simeq A_{ij} \cos \psi_{ij}. \quad (7)$$

Similarly for a quadrature reference signal  $g(t) = \sin \omega_m t$ , we have

$$\begin{aligned}
 \phi_{ij}^2 & \equiv \int_0^T f_{ij}(\tau) \sin \omega_m \tau d\tau \\
 & \simeq A_{ij} \sin \psi_{ij}. \quad (8)
 \end{aligned}$$

From the correlation outputs  $\phi_{ij}^1$  and  $\phi_{ij}^2$ ,  $\psi_{ij}$  is recovered as

$$\psi_{ij} = \tan^{-1} \frac{\phi_{ij}^2}{\phi_{ij}^1}. \quad (9)$$

Note the cancellation of the term  $A_{ij}$ , which contains the nonuniform reflectance coefficient  $R_{ij}$ . Since  $\psi$  is a predetermined monotonic function of  $\theta$  (Fig. 3), the beam angle  $\theta_{ij}$  observed at  $(i, j)$  is recovered as

$$\theta_{ij} = \psi^{-1}(\psi_{ij}). \quad (10)$$

Finally, from Eq. (2) we obtain a depth map  $h_{ij}$  of the object as

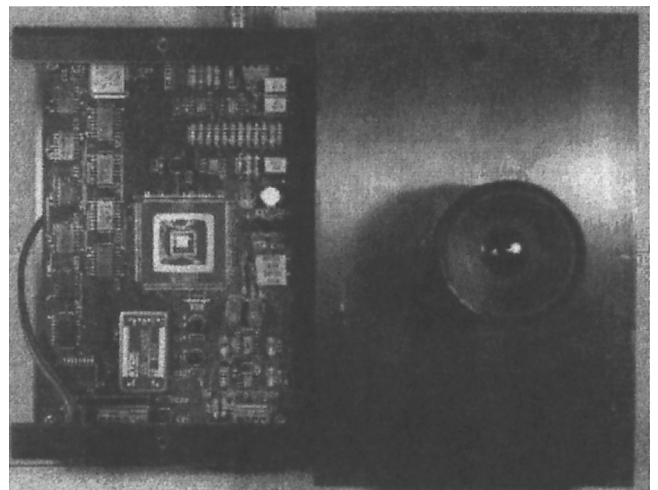


Fig. 5. Photograph of the 64x64-pixel CIS camera module. The CIS chip is mounted at the center of the printed circuit board.

$$h_{ij} = \frac{L}{\frac{\Delta x}{F} i + \frac{1}{\tan \theta_{ij}}} = \frac{L}{\frac{\Delta x}{F} i + \frac{1}{\tan \psi^{-1}(\psi_{ij})}}, \quad \dots (11)$$

where  $\Delta x$  denote the pixel spacing of the CIS, and  $F$  and  $L$  are the same as defined in Eq. (2). In this way,  $h_{ij}$  is obtained from just a single frame pair of quadrature correlation images  $\phi_{ij}^1, \phi_{ij}^2$  without any disturbance by the background illumination  $I_{ij}^0(t)$  and nonuniform reflectance  $R_{ij}$ .

### 3. Experimental System

**3.1 Operation** We implemented an experimental sensing system using a 64x64-pixel CIS chip. Fig. 4 shows the experimental system. The phase shift  $\psi(\theta)$  of the modulated sheet beam as a monotonic function of the beam angle  $\theta$  was realized as follows. The

scanning mirror (General Scanning Inc. XY30M3S + MINISAX) is driven by a controller (General Scanning Inc. SC2000) according to a program loaded from a personal computer. The mirror outputs an analog signal whose voltage is linear to its angular position (i.e. beam angle  $\theta$ ), which is input to a phase shifter to produce phase shift on the modulation carrier proportionally to the input voltage. This phase-shifted carrier is input to a laser diode driver (Wavelength Electronics LTI-4502, maximum current: 200mA) to modulate the sheet beam from a laser diode (Hitachi HL6322, 15mW).

In order to synchronize the CIS, scanning mirror and ADC board, the end-of-frame signal of the CIS is used to trigger both the scan program and A/D conversion. After one scan of the sheet beam, the CIS produces a correlation image frame, which is A/D converted and processed for depth map reconstruction on a workstation. The image frame of the CIS is read out by accessing each pixel in a raster-scan manner over a frame period  $T$ . Since A/D conversion of one pixel output is done within a readout access time of the next pixel (= one pixel clock cycle), it takes almost only one frame period  $T$  to finish A/D converting the whole image. Image acquisition is repeated twice using quadrature reference signals one after another.

**3.2 Correlation Image Sensor** The  $64 \times 64$ -pixel CIS VLSI chip was fabricated with a CMOS process provided by VDEC.<sup>†</sup> The pixel spacing of this chip is  $\Delta x = 60 \mu\text{m}$ . The correlation performance and test applications of this sensor have been reported elsewhere<sup>(9)(10)</sup>. Fig. 5 shows the photograph of the CIS camera. This sensor can produce correlation with only one reference signal at one time, which forces the system to take two frames to obtain an quadrature correlation image pair. It will be possible, however, to obtain a correlation image pair in just a single frame interval by employing a two-channel CIS that can produce correlation with two reference signals at the same time, which is currently being developed in our laboratory.

#### 4. Experimental Results

We carried out experiments on the measurement system shown in Fig. 4 using 2kHz modulation and reference signals all the time. The phase function  $\psi(\theta)$  was designed to vary from 0 to  $2\pi$  over a scan:

$$\psi(\theta) = 2\pi \frac{\theta - \theta_0}{\theta_1 - \theta_0}, \dots\dots\dots (12)$$

where  $[\theta_0, \theta_1]$  denotes the range of the beam angle  $\theta$ . Assuming a uniform scan speed on the CIS image plane, the phase shift that occurs within a sweep of one pixel is  $\frac{2\pi}{64} = 0.098$ , which can be considered small enough to satisfy the assumption  $\psi(\theta(t)) \simeq \psi_{ij}$  for  $t \in [t_{ij}^1, t_{ij}^2]$  in Sec. 2. Furthermore, the setting of  $t_{ij}^2 - t_{ij}^1 \approx \frac{1}{30 \times 64}$  s and  $\omega_m = 2\pi \times 2$  kHz rad validates Eq. (7) since it satisfies  $\omega_m(t_{ij}^2 - t_{ij}^1) \simeq 2\pi$  and hence  $\text{sinc } \omega_m(t_{ij}^2 - t_{ij}^1) \simeq 0$  and  $\text{sinc } \frac{\omega_m}{2}(t_{ij}^2 - t_{ij}^1) \simeq 0$ , despite not satisfying

<sup>†</sup>VLSI Design and Education Center, University of Tokyo. URL: <http://www.vdec.u-tokyo.ac.jp/>.

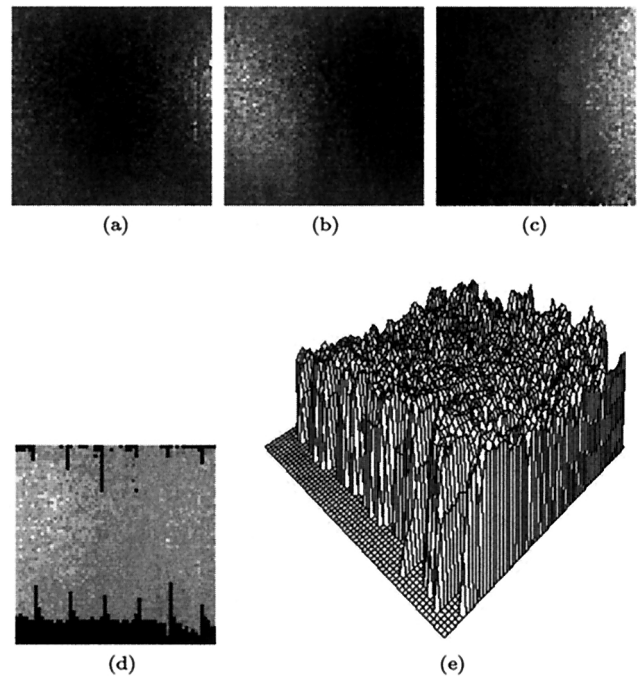


Fig. 6. Measurement result for a parallel flat surface. (a)(b) Quadrature correlation image pair  $\phi_{ij}^1, \phi_{ij}^2$ . (c) Demodulated phase  $\psi_{ij}$ . (d) Reconstructed depth map  $h_{ij}$ . (e) 3-d representation of the depth map. Only the top part of the object is shown. The same description of (a)-(e) is used in Figs. 7-10.

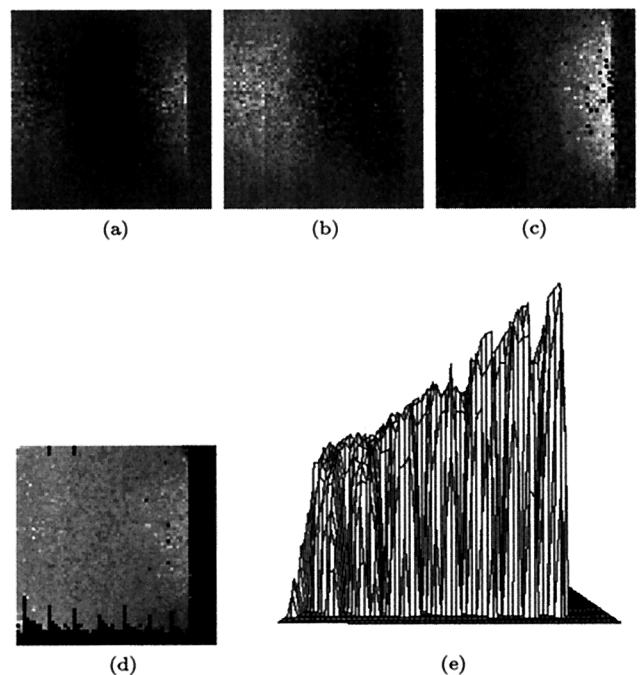


Fig. 7. Measurement result for a slanted flat surface.

$\frac{\omega_m}{2\pi}(t_{ij}^2 - t_{ij}^1) \gg 1$  as claimed in Sec. 2.

Calibration was done by a simple method—taking the cross section image of the laser sheet beam projected onto a flat plane with the CIS for several beam angles, drawing the path of the sheet beam onto graph paper

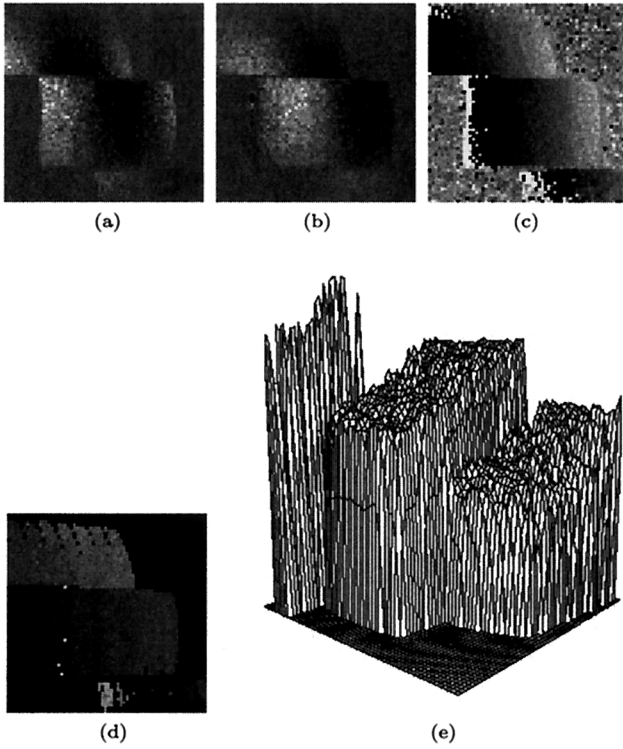


Fig. 8. Measurement result for a staircase-like surface. The actual step pitch of the object is about 18 mm.

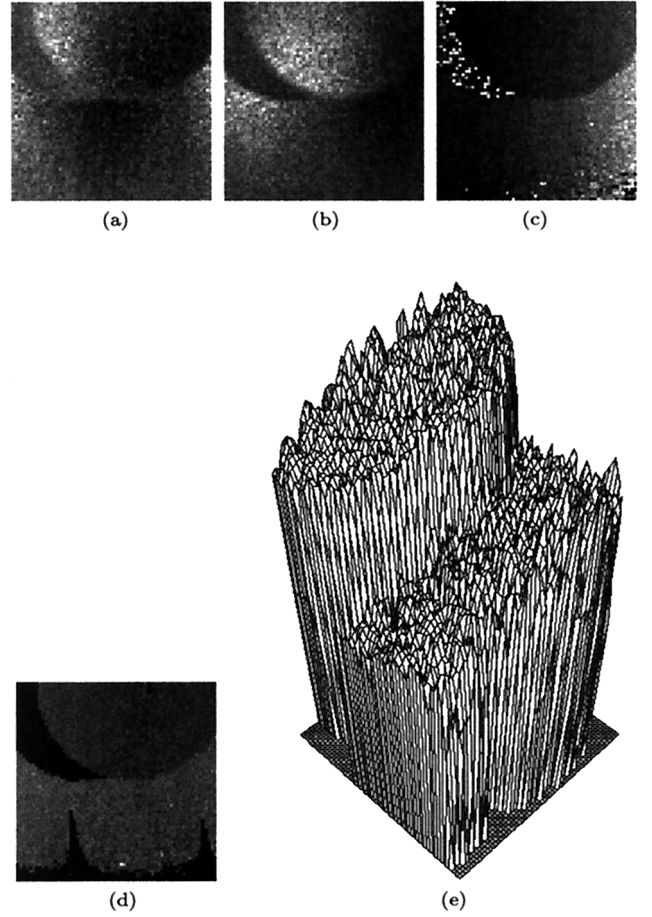


Fig. 9. Measurement result for an object with a circular step edge. The actual step pitch of the object is about 18 mm.

by hand, and calculating the geometrical parameters of the measurement system using two different positions of the flat plane.

#### 4.1 Range Measurement of Various Objects

Figs. 6–10 show the results of range measurement for flat surfaces and objects with step edges. The 3-D plots show that the actual shape of the object surface is successfully recovered.

**4.2 Accuracy** To evaluate the accuracy of the experimental measurement system, we measured a flat surface placed parallel to the CIS at several depth positions. Table 1 lists average measured depth over pixels, systematic error and standard deviation over pixels, under the system setting of  $L = 453$  mm and  $F = 17$  mm. We should note that although some systematic error is still present, the standard deviation is kept below 1% in all the measurement settings.

We compared these results with predicted values based on the formula

$$\sigma_h^2 \leq \left(\frac{\partial h_{ij}}{\partial L}\right)^2 \sigma_L^2 + \left(\frac{\partial h_{ij}}{\partial F}\right)^2 \sigma_F^2 + \left(\frac{\partial h_{ij}}{\partial \theta_{ij}}\right)^2 \left[ \sigma_{PAR}^2 + p^2 \left( \sigma_{SYS}^2 + \frac{2}{r_{SNR}^2} \right) \right], \quad (13)$$

which is derived in Appendix 1. Here  $\sigma_h^2$ , the error variance of depth  $h_{ij}$ , is associated with the error variance of the baseline length  $L$  ( $\sigma_L^2$ ); that of the effective focal length  $F$  ( $\sigma_F^2$ ); that of the beam angle  $\theta_{ij}$  due to the  $\theta_{ij}$ - $\psi_{ij}$  relationship parameters ( $\sigma_{PAR}^2$ ); that of the modulation phase  $\psi_{ij}$  due to nonideal system settings

( $\sigma_{SYS}^2$ ) such as error in the angular position signal from the scanning mirror, or in the phase shift generated by the shifter; and the power signal-to-noise ratio (SNR) of the CIS,  $r_{SNR}^2$ . the parameter  $p$ , defined in Eq. (A5), is equal to  $(\theta_1 - \theta_0)/2\pi$  in terms of Eq. (12). Among these error sources  $r_{SNR}^2$  contributes to deviation over pixels, where as the others contribute to systematic error.

These error parameters were assigned specific values as follows.  $\sigma_L$  and  $\sigma_F$  were empirically found from calibration as

$$\sigma_L = 2 \text{ [mm]}, \quad \sigma_F = 0.5 \text{ [mm]}.$$

The slope  $p$  was determined from the actual scanning range of the sheet beam  $[\theta_0, \theta_1] = [45^\circ, 52^\circ]$ :

$$p = 1.9 \times 10^{-2} \text{ [rad/rad]}.$$

$\sigma_{SYS}$  was set to half the resolution of the phase shifter ( $= 2\pi/32$  rad at 2 kHz), while  $\sigma_{PAR}$  was roughly assumed to be 5% of the total scanning range:

$$\sigma_{SYS} = \frac{2\pi}{32 \times 2} = 9.8 \times 10^{-2} \text{ [rad]},$$

$$\sigma_{PAR} = 0.05 \times 7 \times \frac{\pi}{180} = 6.1 \times 10^{-3} \text{ [rad]}.$$

The SNR of the CIS output was experimentally found to be about 10 dB at 2 kHz, dominated by fixed-pattern

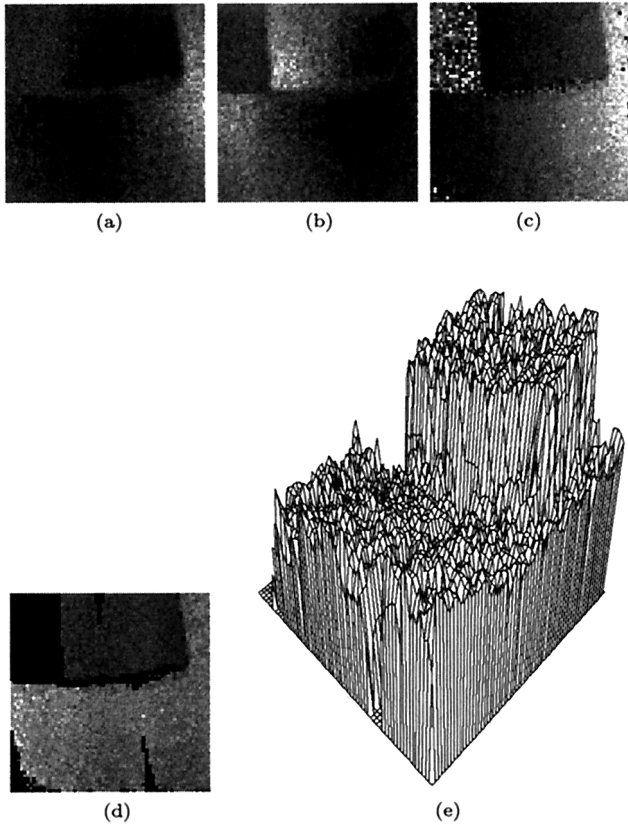


Fig. 10. Measurement result for an object with a rectangular step edge. The actual step pitch of the object is about 18 mm.

noise:

$$r_{SNR}^2 = 10.$$

At a pixel  $(i, j)$  that observes a depth  $h_{ij} = 500$  mm for a beam angle  $\theta_{ij} = 50^\circ$ , the contribution of each error source to  $h_{ij}$  is computed via Eqs. (A2)–(A4), with the actual system settings in the experiment  $L = 453$  mm and  $F = 17$  mm, as

$$\begin{aligned} \left| \frac{\partial h_{ij}}{\partial L} \right| \sigma_L &= 2.2 \text{ [mm]}, & \left| \frac{\partial h_{ij}}{\partial F} \right| \sigma_F &= 1.1 \text{ [mm]}, \\ \left| \frac{\partial h_{ij}}{\partial \theta_{ij}} \right| \sigma_{PAR} &= 5.7 \text{ [mm]}, \\ \left| \frac{\partial h_{ij}}{\partial \theta_{ij}} \right| p \sigma_{SYS} &= 1.8 \text{ [mm]}, \\ \left| \frac{\partial h_{ij}}{\partial \theta_{ij}} \right| p \frac{\sqrt{2}}{r_{SNR}} &\leq 2.5 \text{ [mm]}, \end{aligned}$$

which are all squared and add up to give the error standard deviation of  $h_{ij}$ :

$$\sigma_h \leq 6.9 \text{ [mm]}.$$

The systematic error can be predicted by excluding the contribution of  $r_{SNR}^2$  as

$$\sigma'_h = 6.5 \text{ [mm]}.$$

In view of these values, the systematic error at the

Table 1. Results of accuracy evaluation for a flat surface facing parallel to the CIS in the 450–550mm depth.

Object depth	(mm)	450	500	550
Average measured depth	(mm)	446.4	496.3	542.7
Systematic error	(mm)	−3.6	−3.7	−7.3
(Relative to depth)	(%)	0.8	0.74	1.3
Standard deviation among pixels	(mm)	3.4	3.1	4.5
(Relative to depth)	(%)	0.76	0.62	0.81

depth of 500 mm in Table 1 (−3.7 mm) stays within the predicted value (6.5 mm), whereas the standard deviation (3.1 mm) is kept close to the predicted bound (2.5 mm).

**4.3 Effect of Background Illumination and Nonuniform Surface Reflectance** We tested the range finding system under background illumination and nonuniform surface reflectance of the object. We used a halogen lamp projecting an oblique stripe grid pattern as background illumination. The laser sheet beam was concentrated to the middle portion of the imaging area in this experiment. Fig. 11 shows the results for a flat object with uniform surface reflectance facing parallel to the CIS camera. It allows us to observe the effect of the background illumination alone. The intensity image in Fig. 11(a) taken by the CIS camera exhibits the oblique grid pattern projected by the background illumination source. However, nothing like this grid pattern can be observed in the quadrature correlation images in Figs. 11(b)(c) thanks to temporal correlation. Hence, as shown in Fig. 11(d), the object was reconstructed as a smooth surface with as small fluctuation as about 1 mm except the overall curve, which we consider to have resulted from insufficient calibration of the measurement system in this experiment.

To examine the effect of nonuniform surface reflectance, we used a flat object with a vertical stripe grid pattern on its surface. Fig. 12 shows the results for this nonuniform object obtained under the same background illumination as in Fig. 11. Again, the oblique grid pattern observed in the intensity image in Fig. 12(a) is removed in the quadrature correlation images in Figs. 12(b)(c). Instead Figs. 12(b)(c) show a vertical grid pattern, which resulted from the nonuniform surface reflectance. However, this grid pattern is removed in the reconstructed 3-d plot in Fig. 12(d) thanks to arctangent operation. The fluctuation of the reconstructed surface was found to be about 4 mm, a little larger than in Fig. 11(d), which we attribute to a lower signal level (i.e. lower SNR) of the correlation outputs for dark stripes of the object.

## 5. Discussion

**5.1 Comparison with Other VLSI Range Finders** Table 2 summarizes the performance of (a) the proposed range finder along with that of other VLSI range finders by (b) Gruss *et al.*, (c) Kang *et al.* and (d) Yokoyama *et al.* The frame rate of our range finder can be easily increased by increasing the pixel clock

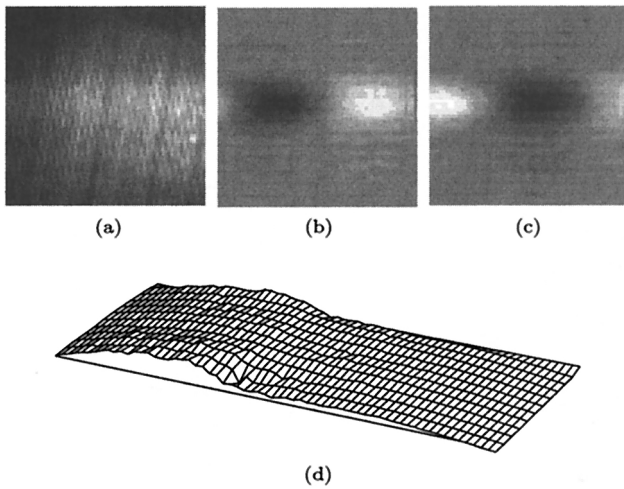


Fig. 11. 3-d reconstruction results in the presence of background illumination. An oblique stripe grid pattern was projected onto a flat surface of uniform reflectance. (a) Intensity image output of the CIS camera. (b)(c) Quadrature correlation image pair  $\phi_{ij}^1, \phi_{ij}^2$ . (d) 3-d plot of depth map  $h_{ij}$ . Only the middle portion of the imaging area is plotted.

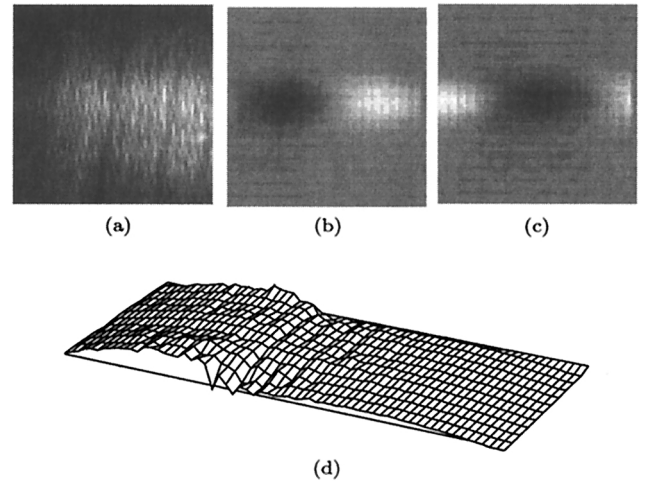


Fig. 12. 3-d reconstruction results in the presence of both background illumination and nonuniform reflectance. A flat surface with a vertical grid pattern was used as an object of nonuniform surface reflectance while the same pattern as in Fig. 11 was projected as background illumination. (a) Intensity image output of the CIS camera. (b)(c) Quadrature correlation image pair  $\phi_{ij}^1, \phi_{ij}^2$ . (d) 3-d plot of depth map  $h_{ij}$ .

frequency. The bottleneck will be the scan speed of the sheet beam. In this case, the modulation frequency  $\omega_m$  of the sheet beam must be increased to ensure the condition  $\frac{\omega_m}{2\pi}(t_{ij}^2 - t_{ij}^1) \gg 1$  claimed in Sec. 2.

**5.2 Accuracy Improvement** With regard to accuracy, the proposed range finder has not yet shown as comparable performance as (c) and (d). For overall accuracy improvement in our system,  $\sigma_\theta^2$  in Eq. (13) must be reduced firstly. This can be done by

- (1) increasing  $r_{SNR}^2$  (= improving the SNR of the CIS),
- (2) decreasing  $\sigma_{PAR}^2$  (= improving the knowledge of parameters  $p, q$  in the  $\theta_{ij}$ - $\psi_{ij}$  relationship in Eq. (A5)),
- (3) decreasing  $\sigma_{SYS}^2$  (= improving reliability of the scanner position signal and the phase shifter), or
- (4) decreasing the slope parameter  $p$  in Eq. (A5) (= increasing the amount of total phase shift during a scan).

The last approach is quite effective since it easily suppresses the error contribution from  $r_{SNR}^2$  and  $\sigma_{SYS}^2$  to  $\sigma_\theta^2$ , as illustrated in Fig. 13. Decreasing  $p$ , on the other hand, will lead to increase in the amount of total phase shift during a scan beyond  $2\pi$  to  $4\pi$  or more. In this case, phase unwrapping should be employed on the demodulated phase map due to  $2\pi$  ambiguities, as shown in Fig. 13(b). It should also be noted that this over- $2\pi$  phase shift should not violate the condition of nearly constant  $\psi_{ij}$  at each pixel, which was claimed in Sec. 2.

**5.3 Increase of Spatial Resolution** For a future CIS with higher spatial resolution than the current  $64 \times 64$  resolution, attention should be paid to:

- (1) The modulation frequency  $\omega_m$  of the sheet

Table 2. Comparison of the proposed range finder with other VLSI range finders.

	This sensor	Gruss <i>et al.</i>	Kang <i>et al.</i>	Yokoyama <i>et al.</i>
# of pixels	$64 \times 64$	$32 \times 28$	$6 \times 6$	$24 \times 24$
Frame rate (Hz)	30	100	150	30
Accuracy (mm)	$-7.3 \pm 4.5$	N.A.	$\pm 1.1$	$\pm 0.024$

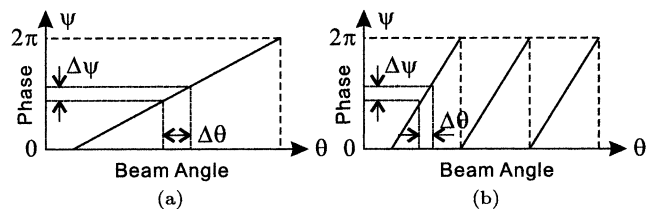


Fig. 13.  $\theta_{ij}$ - $\psi_{ij}$  relationship for (a) larger, and (b) smaller values of the slope parameter  $p = (\theta_1 - \theta_0)/2\pi$ . A smaller  $p$  suppresses the error in demodulated phase  $\psi_{ij}$  in the recovery of beam angle  $\theta_{ij}$ , while introducing some amount of phase wrapping.

beam must be high enough to satisfy  $\frac{\omega_m}{2\pi}(t_{ij}^2 - t_{ij}^1) \gg 1$  as pointed out in Sec. 5.1, since increase in spatial resolution leads to shorter sweeping time of the stripe image.

- (2) The modulation phase  $\psi_{ij}$  must be detected with sufficient resolvability over the imaging area. This can be realized by decreasing the parameter  $p$  in Eq. (A5), although it introduces the problem of phase unwrapping as discussed in Sec. 5.2.

## 6. Conclusion

We proposed a light-stripe range finding system using the correlation image sensor. The key idea of our system

is to encode the beam angle in the phase of the modulated sheet beam and demodulate the phase using the correlation image sensor. The depth map can be reconstructed from a pair of correlation images using quadrature reference signals. The quadrature detection principle removes the effect of background illumination and surface reflectance nonuniformity of the object.

We implemented the sensing system using a 64×64-pixel CMOS CIS chip, and succeeded in the reconstruction of depth maps from a single frame pair of correlation images under the frame rate of 30 Hz. We achieved less than 1% of variation in reconstructed depth maps for 450–550 mm range, and showed robustness to background illumination and nonuniform surface reflectance. We expect that our sensor is particularly useful for range measurement in non-ideal environments such as outdoors under the sunlight.

## Appendix

### 1. Error Analysis

The error variance of depth  $h_{ij}$ , denoted by  $\sigma_h^2$ , is derived by applying the law of error propagation to Eq. (11):

$$\sigma_h^2 = \left(\frac{\partial h_{ij}}{\partial L}\right)^2 \sigma_L^2 + \left(\frac{\partial h_{ij}}{\partial F}\right)^2 \sigma_F^2 + \left(\frac{\partial h_{ij}}{\partial \theta_{ij}}\right)^2 \sigma_\theta^2, \quad (\text{A1})$$

where  $\sigma_L^2$ ,  $\sigma_F^2$  and  $\sigma_\theta^2$  are the error variances of  $L$ ,  $F$  and  $\theta_{ij}$ , respectively, and the partial derivatives are given by

$$\frac{\partial h_{ij}}{\partial L} = \frac{h_{ij}}{L}, \quad \dots \quad (\text{A2})$$

$$\frac{\partial h_{ij}}{\partial F} = \frac{h_{ij}}{F} \left(1 - \frac{h_{ij}}{L \tan \theta_{ij}}\right), \quad \dots \quad (\text{A3})$$

$$\frac{\partial h_{ij}}{\partial \theta_{ij}} = \frac{h_{ij}^2}{L \sin^2 \theta_{ij}}. \quad \dots \quad (\text{A4})$$

The term containing  $\sigma_\theta^2$  in Eq. (A1) results from the error that occurs in both encoding and decoding the beam angle  $\theta_{ij}$ , whereas the other terms are related to accuracy of geometrical setting and calibration.

The error in  $\theta_{ij}$ , denoted by  $\Delta\theta_{ij}$ , is examined from the linear relationship between  $\theta_{ij}$  and the modulation phase  $\psi_{ij}$

$$\theta_{ij} = p\psi_{ij} + q, \quad \dots \quad (\text{A5})$$

where  $p = (\theta_1 - \theta_0)/2\pi$  and  $q = \theta_0$  in terms of Eq. (12).  $\Delta\theta_{ij}$  is derived by approximating Eq. (A5) to first order:

$$\Delta\theta_{ij} \simeq \psi_{ij}\Delta p + p\Delta\psi_{ij} + \Delta q, \quad \dots \quad (\text{A6})$$

where  $\Delta\psi_{ij}$ ,  $\Delta p$  and  $\Delta q$  are the errors in  $\psi_{ij}$ ,  $p$  and  $q$ , respectively. The right hand side of Eq. (A6) is divided into two parts:  $\psi_{ij}\Delta p + \Delta q$  and  $p\Delta\psi_{ij}$ . For the first part, which results from the error in parameters  $p$ ,  $q$ , let us denote its variance by  $\sigma_{PAR}^2$ . The second part, which consists of the error in the modulation phase  $\psi_{ij}$ , has two kinds of independent error sources:

- (1) Detection error of  $\psi_{ij}$  by the CIS (variance

$$\sigma_{CIS}^2).$$

- (2) Other error sources such as error in the position signal  $\theta_{ij}$  from the scanning mirror, or in the phase shift  $\psi_{ij}$  generated from  $\theta_{ij}$  (variance  $\sigma_{SYS}^2$ ).

Thus, the error variance  $\sigma_\theta^2 = E[(\Delta\theta_{ij})^2]$  is expressed as the sum of these error variances:

$$\sigma_\theta^2 = \sigma_{PAR}^2 + p^2(\sigma_{CIS}^2 + \sigma_{SYS}^2). \quad \dots \quad (\text{A7})$$

The error variance  $\sigma_{CIS}^2$  is further examined as follows. Let the quadrature correlation output pair of the CIS,  $\phi_{ij}^1, \phi_{ij}^2$ , be expressed as

$$\phi_{ij}^1 = A_{ij} \cos \psi_{ij} + \Delta\phi_{ij}^1, \quad \dots \quad (\text{A8})$$

$$\phi_{ij}^2 = A_{ij} \sin \psi_{ij} + \Delta\phi_{ij}^2, \quad \dots \quad (\text{A9})$$

where  $\Delta\phi_{ij}^1, \Delta\phi_{ij}^2$  denote error terms. These errors lead to the error  $\Delta\overline{\psi_{ij}}$  in the demodulated phase  $\psi_{ij}$  as

$$\tan(\psi_{ij} + \Delta\overline{\psi_{ij}}) = \frac{\phi_{ij}^2}{\phi_{ij}^1}. \quad \dots \quad (\text{A10})$$

Approximating this relationship to first order and rearranging terms give an expression for  $\Delta\overline{\psi_{ij}}$ :

$$\Delta\overline{\psi_{ij}} \simeq \rho_{ij} \cos(\psi_{ij} - \delta_{ij}), \quad \dots \quad (\text{A11})$$

where

$$\rho_{ij} = \sqrt{\left(\frac{\Delta\phi_{ij}^1}{A_{ij}}\right)^2 + \left(\frac{\Delta\phi_{ij}^2}{A_{ij}}\right)^2}, \quad \dots \quad (\text{A12})$$

$$\delta_{ij} = \tan^{-1} \frac{\Delta\phi_{ij}^2}{-\Delta\phi_{ij}^1}. \quad \dots \quad (\text{A13})$$

The expectation of  $\left(\frac{\Delta\phi_{ij}^1}{A_{ij}}\right)^2$  and  $\left(\frac{\Delta\phi_{ij}^2}{A_{ij}}\right)^2$  is replaced by the reciprocal of the maximum signal-to-noise ratio (SNR) of the CIS output,  $r_{SNR}^2$ :

$$\frac{E[(\Delta\phi_{ij}^1)^2]}{A_{ij}^2} = \frac{E[(\Delta\phi_{ij}^2)^2]}{A_{ij}^2} = \frac{1}{r_{SNR}^2}. \quad \dots \quad (\text{A14})$$

Thus, from Eqs. (A11), (A12) and (A14),  $\sigma_{CIS}^2 \equiv E[(\Delta\overline{\psi_{ij}})^2]$  is evaluated as

$$\sigma_{CIS}^2 \leq E[\rho_{ij}^2] = \frac{2}{r_{SNR}^2}. \quad \dots \quad (\text{A15})$$

Substituting Eqs. (A7) and (A15) into Eq. (A1), we obtain

$$\sigma_h^2 \leq \left(\frac{\partial h_{ij}}{\partial L}\right)^2 \sigma_L^2 + \left(\frac{\partial h_{ij}}{\partial F}\right)^2 \sigma_F^2 + \left(\frac{\partial h_{ij}}{\partial \theta_{ij}}\right)^2 \left[\sigma_{PAR}^2 + p^2 \left(\frac{2}{r_{SNR}^2} + \sigma_{SYS}^2\right)\right]. \quad (\text{A16})$$

(Manuscript received June 20, 2000, revised February 16, 2001)

## References

- (1) R.A.Jarvis, "A perspective on range finding techniques for computer vision," *IEEE Trans. Pat. Anal. Mach. Intell.*, vol.**PAMI-5**, no.2, pp.122–139, 1983.
- (2) A.Gruss, L.R.Carley and T.Kanade, "Integrated sensor and range-finding analog signal processor," *IEEE J. Solid-State Circuits*, vol.**26**, no.3, pp.67–71, 1991.
- (3) S.H.Kang, S.S.Lee, K.S.Hong and O.H.Kim, "Digital range imaging VLSI sensor," *IEICE Trans. Inf. & Syst.*, vol.**E77-D**, no.11, pp.1302–1305, 1994.
- (4) A.Yokoyama, K.Sato, T.Yoshigahara and S.Inokuchi, "Realtime range imaging using adjustment-free photo-VLSI—silicon range finder," in *IEEE Int. Conf. Intell. Robots and Systems*, pp.1751–1758, 1994.
- (5) S. Ando, T. Nakamura and T. Sakaguchi, "Ultrafast correlation image sensor: concept, design and applications," in *Proc. Transducers '97*, pp. 307–310, Chicago, IL, 1997.
- (6) S. Ando, T. Nakamura and T. Sakaguchi, "Ultrafast correlation image sensor: concept, design and applications," in *Proc. IEEE Workshop on CCD and Advanced Image Sensors*, Bruges, Belgium, 1997.
- (7) T. Sakaguchi, T. Nakamura and S. Ando, "Ultrafast correlation image sensor: fabrication and experiments with 8×8 pixel model," in *Tech. Digest of 15th Sensor Symp.*, pp. 111–114, Kawasaki, Japan, 1997.
- (8) A. Kimachi, R. Imaizumi and S. Ando, "Intelligent image sensor with a vibratory mirror mimicking involuntary eye movement," in *Tech. Digest of 16th Sensor Symp.*, pp. 171–176, Kawasaki, Japan, 1998.
- (9) A. Kimachi and S. Ando, "Time-domain correlation image sensor: first CMOS realization and evaluation," in *Proc. Transducers '99*, pp. 958–961, Sendai, Japan, 1999.
- (10) S. Ando and A. Kimachi, "Time-domain correlation image sensor: first CMOS realization of demodulator pixels array," in *Proc. IEEE Workshop on CCD and Advanced Image Sensors*, pp. 33–36, Karuizawa, Japan, 1999.

**Akira Kimachi** (Member) received B.E. M.E. and Ph.D.



degrees in mathematical engineering and information physics from the University of Tokyo, in 1993, 1995 and 1999, respectively. From 1999 to 2001 he was an assistant professor at the Department of Mathematical Engineering and Information Physics, Graduate School of Engineering, the University of Tokyo. He is currently a lecturer at the Department of Engineering Informatics, Osaka Electro-

Communication University. His research interest is in the area of image sensing, image processing and imaging devices. He is a member of IEEJ, SICE and IEICE.

**Toru Kurihara** (Non-member) received a B.E. degree



in mathematical engineering and information physics from the University of Tokyo in 2000. He is currently a M.E. student at the Department of Information Physics and Computing, Graduate School of Information Science and Technology, the University of Tokyo. His research interest is in the area of image sensing and control engineering.

**Masao Takamoto** (Non-member) received a B.E. degree in mathematical engineering and information physics from the University of Tokyo in 2000. He is currently a M.E. student at the Department of Applied Physics, Graduate School of Engineering, the University of Tokyo. His research interest is in the area of image sensing and applied physics.



**Shigeru Ando** (Member) received B.S., M.E. and Ph.D.



degrees from the University of Tokyo. From 1987 to 1997, he was an associate professor in mathematical engineering and information physics at the University of Tokyo. He is currently a professor at the Department of Information Physics and Computing, Graduate School of Information Science and Technology, the University of Tokyo. His research and teaching activities have been

in the area of smart sensors, vision sensors, auditory sensors, circuits, non-linear signal processing and image processing. He is a member of IEEJ, SICE, IEEE and OSA.